

UC Berkeley

UC Berkeley Previously Published Works

Title

Interconnection of the Antenna Pigment 8-HDF and Flavin Facilitates Red-Light Reception in a Bifunctional Animal-like Cryptochrome

Permalink

<https://escholarship.org/uc/item/743261dh>

Journal

Biochemistry, 59(4)

ISSN

0006-2960

Authors

Oldemeyer, Sabine
Haddad, Andrew Z
Fleming, Graham R

Publication Date

2020-02-04

DOI

10.1021/acs.biochem.9b00875

Supplemental Material

<https://escholarship.org/uc/item/743261dh#supplemental>

Peer reviewed

Interconnection of the Antenna Pigment 8-HDF and Flavin Facilitates Red Light Reception in a Bifunctional Animal-like Cryptochrome

*Sabine Oldemeyer ^{*a,b}, Andrew Z. Haddad ^c, Graham R. Fleming ^{a,b,d}*

*^aDepartment of Chemistry, University of California, Berkeley, CA 94720,
United States*

*^bMolecular Biophysics and Integrated Bioimaging Division, Lawrence Berkeley
National Laboratory, Berkeley, California 94720, United States*

*^cEnergy Technologies Area, Lawrence Berkeley National Laboratory,
Berkeley, California 94720, United States*

^dKavli Energy Nanoscience Institute, Berkeley CA 94720, United States

ABSTRACT. Cryptochromes are ubiquitous flavin-binding light sensors closely related to DNA repairing photolyases. The animal-like cryptochrome *CraCRY* from the green alga *Chlamydomonas reinhardtii* challenges the paradigm of cryptochromes as pure blue-light receptors by acting as a (6-4) photolyase, using 8-hydroxy-5-deazaflavin (8-HDF) as a light harvesting antenna with a 17.4 Å distance to flavin and showing spectral sensitivity up to 680 nm. The expanded action spectrum is attributed to the presence of the flavin neutral radical (FADH•) in the dark, despite a rapid FADH• decay observed in vitro in samples exclusively carrying flavin. Herein, the red-light response of *CraCRY* carrying flavin and 8-HDF was studied, revealing a 3-fold prolongation of the FADH• life-time in the presence of 8-HDF. Millisecond time-resolved UV-vis spectroscopy showed the red light-induced formation and decay of an absorbance band at 458 nm concomitant to flavin reduction. Time-resolved FTIR spectroscopy and density functional theory attributed these changes to the deprotonation of 8-HDF, challenging the paradigm of 8-HDF being permanently deprotonated in photolyases. FTIR spectra showed changes in the hydrogen bonding network of asparagine 395, a residue suggested to indirectly control the flavin protonation, indicating the involvement of N395 in the stabilization of FADH•. Fluorescence spectroscopy revealed a decrease in energy transfer efficiency of 8-HDF upon flavin reduction, possibly linked to the 8-HDF deprotonation. The discovery of the interdependence of flavin and 8-HDF beyond energy transfer processes highlights the essential role of

the antenna, introducing a new concept enabling *CraCRY* and possibly other bifunctional cryptochromes to fulfill their dual function.

1.INTRODUCTION

Cryptochromes constitute a diverse group of sensory photoreceptors present in all three kingdoms of life and are known to regulate a wide range of processes.¹⁻⁵ They form the cryptochrome/photolyase family, together with photolyases, enzymes responsible for repairing UV-light induced DNA lesions, either cyclobutane-pyrimidine dimers (CPD)⁶ or pyrimidine-(6-4)-pyrimidone photoadducts, (6-4)PP.⁷ Members of this protein family share the highly conserved photolyase homology region (PHR) comprising of 500 residues.¹

The C-terminal α -helical domain of the PHR harbors the light sensing flavin adenine dinucleotide (FAD) chromophore whereas the N-terminal α/β domain in some cases binds a light harvesting pigment, commonly known as an antenna chromophore. Antenna chromophores known to date include 5,10-methenyltetrahydrofolate (MTHF)^{8, 9}, 7,8-dimethyl-8-hydroxy-5-deazaflavin (8-HDF)¹⁰⁻¹², flavin mononucleotide (FMN)¹³, 6,7-dimethyl-8-ribityllumazine (DMLR)¹⁴ and FAD in its fully oxidized state (FAD_{ox}).¹⁵ In many cryptochromes and photolyases a C-terminal extension (CCT) with highly varying amino acid composition and length is present and was found in plant and insect cryptochromes to be involved in signaling.^{16, 17}

The Cryptochrome subfamily further diversifies into animal types I and II, plant CRYs and DASH cryptochromes (*Drosophila*, *Arabidopsis*, *Synechocystis*, *Homo*).^{18, 19} The group of animal type II cryptochromes are closely related to (6-4) photolyases and include the animal-like cryptochrome CraCRY or, for short, aCRY, from the green algae *Chlamydomonas reinhardtii*.²⁰ Strikingly, aCRY challenges the paradigm of cryptochromes being exclusively blue light receptors, as it responds *in vivo* to red light up to 680 nm by altering transcript levels for proteins involved in processes such as cell cycle control and chlorophyll and carotenoid biosynthesis.²⁰ As opposed to plant cryptochromes, where the oxidized flavin (FAD_{ox}) is present^{21, 22}, the broadened spectral sensitivity observed in aCRY is rationalized by the non-covalent binding of the flavin neutral radical (FADH•) in the dark form of the receptor (Fig. 1 A).²⁰ The FADH• absorption spectrum was found to be in agreement with the action spectrum of aCRY *in vivo* and structural rearrangements in the protein moiety of aCRY were only found upon formation of the anionic fully reduced state (FADH⁻) as revealed by FTIR spectroscopy and hydrogen/deuterium exchange mass spectrometry on aCRY.²³⁻²⁵

In contrast to other cryptochromes, the lifetime of the FADH• state *in vitro* is not influenced by oxygen levels²⁶⁻²⁸ but strongly sensitive to alterations of the pH. At a pH of 6.9 a lifetime of 1340 s was reported.²³ Neighboring amino acids were proposed to control the pH sensitivity by acting as proton donors.²³ Franz et. al. suggested that the asparagine 395 (N395) in close

proximity to FAD (Fig. 1C) might function as a gatekeeper for a solvent-dependent deprotonation of FADH• and thus indirectly regulate the radical's stability.²⁹ However, an explanation for the short life time of the FADH• *in vitro* as opposed to its permanent presence *in vivo* is not yet available.

In addition to the protein's structural response it was found that in aCRY tyrosine 373 (Y373) is oxidized in ~800 ps³⁰ and forms a long-lived tyrosyl radical (TyrO•) with a life time of 2.6 s upon red light illumination.^{24, 31} TyrO• is stabilized by the formation of a π - π stacking with the neighboring tryptophan 322 (W322).³² Both Y373 and W322 are part of the conserved redox tetrad (Fig.1 C) and are essential for the successful photoreduction.

Interestingly, aCRY was only recently found to have maintained the ability to repair (6-4)PP DNA lesions *in vivo* and to carry the non-covalently bound antenna pigment 8-HDF possibly deprotonated at the 8-hydroxyl group²⁹ which has a pKa value of 6.3³³ (Fig.1 B). The deprotonation was rationalized by the presence of positively charged residues lysine 258 (L258) and arginine 55 (R55) next to the 8-hydroxyl group^{10, 29} (Fig. 1C) as well as the red-shifted absorbance maximum at 448 nm, which is similar to spectra previously found for other 8-HDF-binding photolyases.^{10, 12, 34} In these enzymes, the red-shifted absorbance as opposed to the pigment's absorbance maximum in aqueous solution at 421 nm (Fig. 1A) was explained by a negative solvatochromic effect exhibited by charged species in a non-polar environment such as the protein matrix.³⁵ Previous experiments investigating the red light-response of aCRY *in vitro* were conducted

exclusively on samples without the antenna pigment 8-HDF. The recent discovery of the non-covalent binding of 8-HDF in aCRY raises the question whether it solely serves to increase DNA repair efficiency in the protein's role as a photolyase or whether it may also have an impact on aCRY's function as a red light sensor especially with regard to the formation of the stable tyrosyl radical. In this study, we address this question through use of ms-time-resolved UV/vis spectroscopy, ms-time-resolved infrared spectroscopy, quantum chemical calculations and fluorescence spectroscopy.

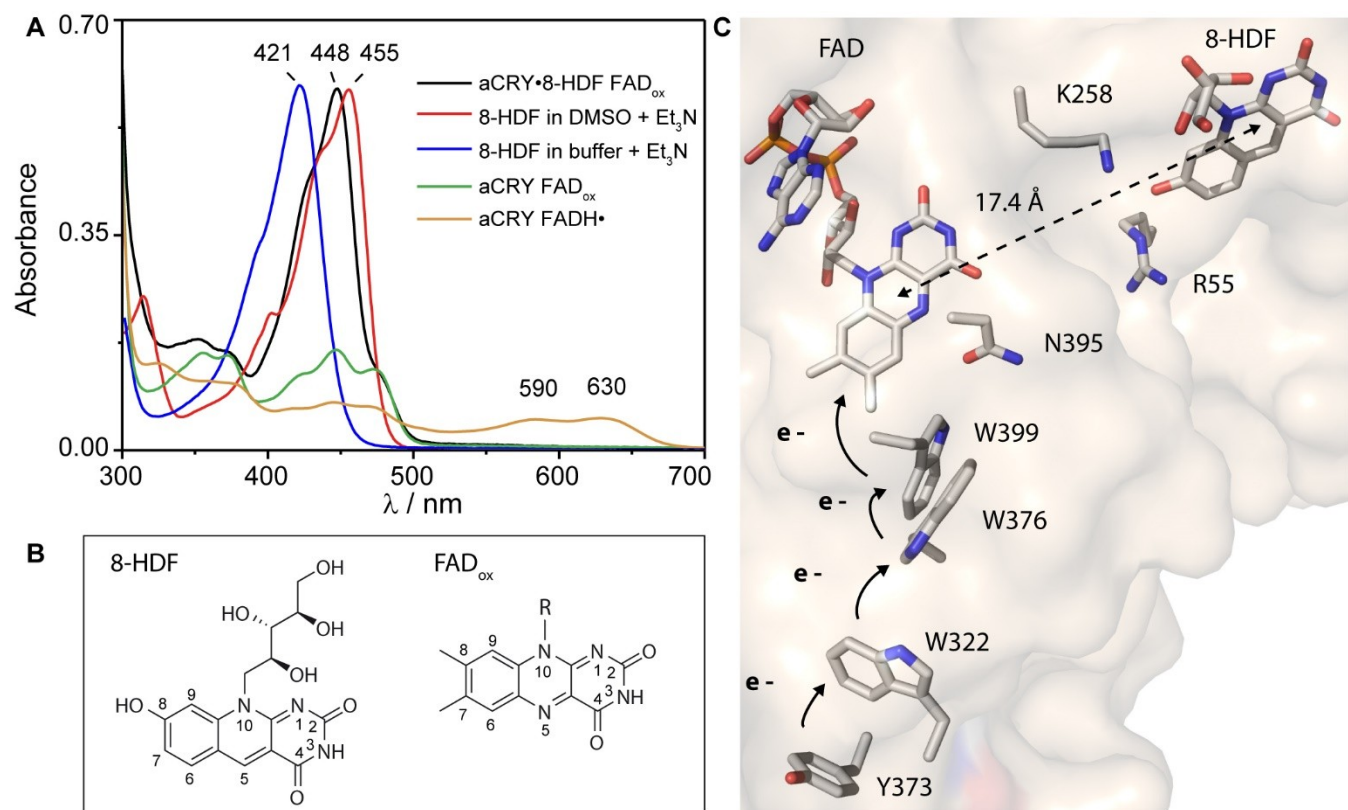


Figure 1. (A) The absorbance of aCRY•8-HDF is compared to aCRY binding carrying FAD_{ox} or FADH•, and 8-HDF in different solvents. aCRY•8-HDF has a

maximum at 448 nm and a shoulder at 473 nm showing the [non-covalent](#) binding of 8-HDF and FAD_{ox}, respectively. (B) Chemical structures of FAD_{ox} and protonated 8-HDF. (C) Tyrosine 373 and the three tryptophans 322, 376 and 399 form the electron transfer tetrad responsible for flavin reduction. Asparagine 395 is proposed to indirectly control the deprotonation of FADH•. Lysine 258 and arginine 55 are suggested to be involved the deprotonation of 8-HDF. The structure is taken from (29).

2. MATERIALS AND METHODS

2.1 Expression and purification of aCRY•8-HDF and aCRY. Wild-type aCRY protein carrying FAD and the antenna chromophore 8-HDF (aCRY•8-HDF) was expressed in *Escherichia coli* BL21(DE3) after transforming the cells with pET28a-aCRY and the cofactor plasmid pCDF-His₆FbiC which encodes for the F0 synthase (7,8-didemethyl-8-hydroxy-5-deazariboflavin synthase) of *Streptomyces coelicolor*. Wild-type aCRY without 8-HDF only carrying FAD (aCRY) was expressed in *Escherichia coli* BL21(DE3) subsequent to the transformation of the cells with pET28a-aCRY. These procedures and the purification of aCRY•8-HDF and aCRY were conducted following published protocols.^{20, 36} The proteins were dissolved in a 50 mM sodium phosphate buffer at pH 7.0 with 100 mM NaCl and 20% (v/v) glycerol after final dialysis. [As a control for the sample homogeneity, a fraction of the sample was further purified using size exclusion chromatography \(Supporting information\).](#)

The chromophore occupancy was determined before and after the size exclusion chromatography by spectrally decomposing an absorbance spectrum of aCRY•-8-HDF according the Beer-Lambert law³⁷, where the absorbance A is given by the product of the path length l , the concentration c and the molar extinction coefficient ϵ . The flavin concentration was calculated using the molar extinction coefficient of oxidized flavin at 450 nm of $11300 \text{ M}^{-1}\text{cm}^{-1}$ ¹³⁸ after scaling an absorbance spectrum of aCRY to the flavin shoulder at 476 nm in the aCRY•8-HDF spectrum (Fig S1). After subtracting the flavin absorbance portion from the aCRY•8-HDF spectrum the molar extinction coefficient of 8-HDF at 448 nm of $37500 \text{ M}^{-1}\text{cm}^{-1}$ ¹³⁵ was used to obtain the 8-HDF concentration. To determine the protein concentration, an absorbance spectrum of a dilution of the aCRY•8-HDF sample was generated and both flavin and 8-HDF contributions were subtracted from the absorbance at 280 nm. Using the molar extinction coefficient of the aCRY protein matrix at 280 nm of $107830 \text{ M}^{-1}\text{cm}^{-1}$ ¹³⁹ the overall protein concentration and chromophore occupancy was determined.

2.2 UV-vis spectroscopy and kinetic experiments. UV-vis spectra were recorded using a UV-2450 spectrometer (Shimadzu). The concentration of each three independent aCRY•8-HDF and aCRY samples were adjusted to an $A_{4487} = 0.6$ and $A_{45048} = 0.3$, respectively, for long-term kinetics. The flavin neutral radical was generated by illuminating aCRY•8-HDF and aCRY for 3 s and 1 s, respectively, using a 473 and 451 nm-LED (Luxeon Star, Lumileds) with intensities of 32 mW/cm^2 at the sample and a full width at half-

maximum (FWHM) of 15 nm. The decay of the flavin neutral radical was recorded at 6302 nm subsequent to the illumination.

2.3 Millisecond Time-resolved UV-Vis Spectroscopy. Three independent samples with a concentration adjusted to an optical density of 0.6 at 448 nm were measured in an HR2000+ spectrometer (Ocean Optics) in a 2x10 mm fluorescence cuvette (Helma). The DH-2000-BAL light source was attenuated by a mesh filter with 35% transmission to prevent photo bleaching of the sample by the probe light. Photo conversion was conducted by two LEDs perpendicularly fastened to the sample holder. A 473 nm-LED (Luxeon Star, Lumileds) with an intensity of 63 mW/cm² (FWHM of 20 nm) and a 632 nm LED (Luxeon Star, Lumileds) with an intensity of 95 mW /cm² (FWHM of 15 nm) at the sample were used for 10 s or 2 s to generate FADH• and FADH-, respectively. During and after illumination a consistent series of spectra was recorded with an integration time of 2 ms and a time resolution of 44 ms. Difference spectra were calculated and summarized on a logarithmic time scale to improve the signal-to-noise ratio using MATLAB (The Mathworks).

2.4 Rapid-scan FTIR spectroscopy. Ultrafiltration was conducted using Vivaspin 500 filter devices (Sartorius, 50 kDa cutoff) to concentrate the proteins to a final OD₄₄₇ of ~25 and OD₄₄₈ of ~32 for aCRY and aCRY•8-HDF, respectively. The samples were washed with 20 mM sodium phosphate buffer three times, pH 7.0, 100 mM NaCl, 1% (v/v) glycerol during centrifugation at 15.000g. A droplet of 2.0 µL sample solution was placed on

a BaF₂ window (20 mm diameter) and kept at 20 °C under atmospheric pressure for up to 20 s for a slight reduction of the water content. An additional BaF₂ window was used to seal the samples forming a well-hydrated film with an absorbance ratio of amide I/water (1650 cm⁻¹) to amide II (1550 cm⁻¹) of 2.4–2.6. An IFS 66/s spectrometer (Bruker) equipped with a photoconductive mercury cadmium telluride (MCT) detector at a spectral resolution of 4 cm⁻¹ was used to perform the rapid-scan experiments. The mirror was set in a double-sided, forward–backward mode to a velocity 160 kHz. The difference spectra were obtained with a long wave pass filter (OCLI) cutting off infrared and visible light above 2256 cm⁻¹.

aCRY•8-HDF and aCRY were pre-illuminated with blue light for 10 s with a 473-nm (aCRY•8-HDF) or 451-nm LED (aCRY) equipped with a diffusion disc and yielding an intensity of 30 and 32 mW/cm² at the sample, respectively. The reference intensity was recorded for 512 scans followed by red light illumination for 3 s with a 632 nm LED with an intensity of 40 mW/cm² at the sample. The first difference spectrum was recorded from 16 ms to 121 ms with a midpoint of 69 ms after the red light illumination, and further 49 spectra were recorded until 1818 s. Subsequently, 4 (aCRY•8-HDF) or 9 (aCRY) single experiments, each time using a fresh and independently prepared sample, were averaged. The experiments were performed at a constant temperature of 10 °C.

2.5 Quantum chemical calculations. The calculation of normal modes and the optimization of the geometry was conducted using density functional

theory (DFT) as implemented in Gaussian16 A03⁴⁰ using Becke's B3LYP hybrid exchange-correlation functional^{41, 42} and the 6-311+G(2d,p) basis set. The B3LYP functional previously yielded results in vibrational frequencies matching the experiment data very well.⁴² A single factor of 0.98 was used to scale the frequencies, as it gave excellent results in calculations of Flavin.⁴³ The line spectrum was folded with Lorentzians with a full width at half maximum of 14 cm⁻¹ as determined for the homogenous broadening of flavin bands.⁴⁴

2.6 Fluorescence spectroscopy. Prior to the experiments, all protein samples were purified by size exclusion chromatography via a PD10 column (GE Healthcare) according to the specifications of the manufacturer to remove unbound chromophore. Samples of aCRY•8-HDF and aCRY were adjusted to the same concentration of FAD_{ox} at 473 nm with $A_{448}=0.65$ and $A_{447}=0.15$, respectively. To ensure the same absorbance of 8-HDF as in the protein sample, the chromophore in 50 mM sodium phosphate buffer, pH 7.0, 100 mM NaCl, 20% (v/v) glycerol and DMSO each with 0.1% Et₃N was set to A_{421} and A_{455} nm=0.5. A Fluorolog-3 spectrofluorometer (Horiba Jobin Yvon) equipped with a CCD camera was used to record emission spectra of the samples. For the comparison of the fluorescence intensities of aCRY•8-HDF, aCRY and 8-HDF solvated in phosphate buffer or DMSO samples were excited at their absorption maxima at 448, 447, 421 and 455 nm respectively, with a bandwidth of 5 nm and a detection time of 0.02 s. To generate aCRY•8-HDF with different flavin oxidation states, FADH• was generated upon 10 s of

illumination at 473 nm and a permanent stabilization of FADH⁻ was achieved upon addition of 10 μM ascorbic acid and 40 s of illumination at 473 nm. The samples were excited at 432 nm with a detection time of 0.02 s. [To test the sample homogeneity, these experiments were repeated with a sample containing 92% and 93% FAD and 8-HDF occupancy, respectively, after an additional size exclusion chromatography \(Supporting information, Fig S2\).](#)

2.7 Calculation of the energy transfer efficiency in aCRY•8-HDF.

The theoretical efficiency of the resonant energy transfer (RET) E was calculated for aCRY•8-HDF with 8-HDF acting as the donor to either FAD_{ox}, FADH• or FADH⁻ as receptors.

$$E = \frac{R_0^6}{R_0^6 + r^6} \quad [1]$$

The Foerster radius R_0 is the distance at which the energy transfer efficiency between the chromophores is 50% and r represents the center-to-center distance of the donor-acceptor pair with a value of 17.4 Å as derived from the structure.²⁹ R_0 was calculated using equation (2):

$$R_0 = 0.211 \left[\frac{\kappa^2 \Phi_D J(\lambda)}{n^4} \right]^{\frac{1}{6}} \quad [2]$$

κ^2 is an orientation factor of the chromophores, representing the angle of the transition dipole moments of donor and acceptor towards each other. An orientation factor of 1.82 was chosen, as calculated for FADH⁻ and 8-HDF in the (6-4) photolyase of *A. nidulans*.⁴⁵ The quantum yield of the donor chromophore in absence of the acceptor is represented by Φ_D and was

determined to be 0.65 for 8-HDF.⁴⁶ $J(\lambda)$ is the overlap integral of the molar extinction coefficient of the acceptor in $\text{nm}^4\text{M}^{-1}\text{cm}^{-1}$ and the normalized emission spectrum of the donor in the absence of the acceptor (Fig. S23) and is listed in Table S251. For the fluorescence spectrum of the donor in absence of the acceptor a spectrum of 8-HDF in phosphate buffer was chosen. n is the refractive index with a value of 1.39 for a protein buffer.⁴⁷

3.RESULTS

The co-expression of wild type aCRY with a plasmid coding for the F0-synthase revealed 8-HDF to be bound as a potential antenna chromophore in the full-length protein.²⁹ To investigate the influence of the additional chromophore on the red light response of the protein, aCRY•8-HDF was successfully expressed and purified carrying both 8-HDF and FAD as confirmed by UV/vis analysis after final cleansing (Fig. 2A). The absorption spectrum of the protein shows a prominent band at 448 nm with a shoulder at 430 nm assigned to 8-HDF. The detection of an additional absorbance band with maxima at 355 and 373 nm as well as a shoulder at 475 nm verifies the presence of protein bound flavin in the oxidized state. The occupancy of 8-HDF and FAD_{ox} in aCRY•8-HDF after the complete purification procedure is ~~determined~~—calculated to be at least 30% and 34%, respectively. After an additional size exclusion chromatography on a fraction of the sample, aCRY•8-HDF with an occupancy of 92% and 93% for FAD and 8-HDF, respectively, was obtained (Fig. S1). Fluorescence spectroscopy conducted on samples before and after the additional chromatography

yielded almost identical results, showing that in the samples with the lower calculated chromophore occupancy FAD and 8-HDF were binding cooperatively to the same proteins. Therefore, for all following experiments, aCRY•8-HDF samples were used without the additional purification step. The molar extinction coefficients of oxidized flavin at 450 nm of $11300 \text{ M}^{-1}\text{cm}^{-1}$ ³⁸ and of 8-HDF at 448 nm of $37500 \text{ M}^{-1}\text{cm}^{-1}$ ³⁵ were used. In order to study the physiologically relevant red light-response in aCRY•8-HDF, FADH• was generated in the sample via illumination at 473 nm for 10 s. The formation of the characteristic absorbance bands at 590 and 630 nm indicated the successful generation of the neutral radical (Fig. 2A).

Previously, it was found that FADH• decays within an hour to FAD_{ox} at a pH of 6.9 in the dark at 20 °C²³, constituting a major distinction from the neutral radical's permanent presence *in vivo*.²⁰ To investigate the effect of the presence of the antenna 8-HDF on the life time of FADH• in aCRY•8-HDF the neutral radical was generated via blue-light illumination at 473 nm for 3 s followed by monitoring the absorbance decay at 630 nm via kinetic measurements at 20°C and pH 7.0 (Fig 2B). Analysis of the decay curves of three independent samples of aCRY•8-HDF with biexponential fits yielded average time constants of 5225 s (72%, ± 510 s) and 284 s (28%, ± 21 s). For comparison the lifetime of FADH• in aCRY was measured in three independent samples under identical conditions except that the sample was illuminated for 1 second at 451 nm. For better visualization, the decay curve of aCRY was scaled by a factor of 0.51. Here, the biexponential fit yielded

averaged time constants of 1469 s (66 %, \pm 120 s) and 156 s (34 %, \pm 15 s). Strikingly, the lifetime of the long and short components in aCRY•8-HDF are 3.5 and 1.8 times longer, respectively, than the lifetime of FADH• found in aCRY.

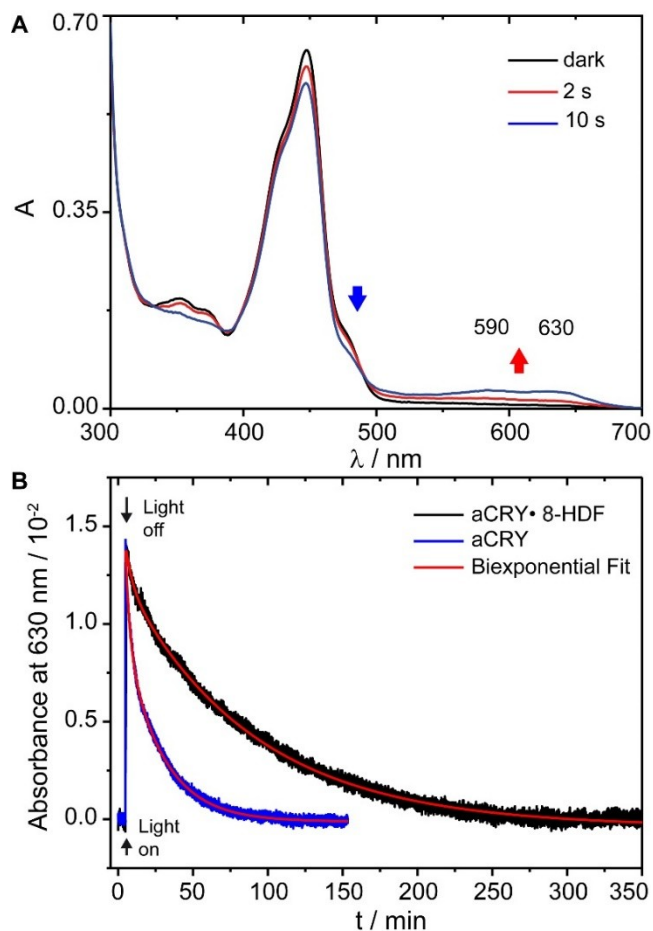


Figure 2. (A) FAD_{ox} is converted to FADH• in aCRY•8-HDF by illumination at 473 nm, shown by the FADH• marker bands at 590 and 630 nm. (B) Comparison of UV-vis long-term kinetics of aCRY•8-HDF and aCRY, scaled by a factor of 0.51. Biexponential fitting yielded time constants of $\tau_1=5225$ s (72%), $\tau_2=284$ s (28%) and $\tau_1=1469$ s (66%), $\tau_2=156$ s (34%) for aCRY•8-HDF

and aCRY, respectively, revealing a 3.5-fold prolongation of the major component of the FADH• life time in aCRY•8-HDF relative to aCRY.

3.1 Effect of 8-HDF on the life-time of TyrO• and FADH• in aCRY•8-HDF. Previously, in aCRY the Y373 was found to form an unusually stable tyrosyl radical (TyrO•) with a life-time of 2.6 s in response to red light, decaying mutually with the FADH•.²⁴ In order to assess whether the presence of the antenna chromophore influences the stability of the radical, the decay of TyrO• and FADH• after red light illumination was analyzed at 20 °C on a millisecond time scale. Difference spectra were calculated by subtracting spectra averaged over 1 s subsequent to illumination from spectra prior to illumination (Fig. 3A). In addition to the marker bands of TyrO• and FADH• at 410 and 630 nm, the spectrum of aCRY•8-HDF shows a band at 458 nm (Fig 3A, *inset*), which is not observed in the difference spectrum of aCRY (Fig 3A), suggesting that it originates from 8-HDF. To analyze the decay of TyrO• and FADH•, changes in absorbance at 385-425 nm and 550-605 nm were integrated and fitted monoexponentially, yielding time constants of 2.0 s for both processes (Fig. 3B). TyrO• and FADH• both decay 23% faster than in aCRY ($\tau = 2.6$ s), respectively, yielding similar time constants (2.3 s for TyrO• and FADH•) as found in the aCRY-C482A mutant²⁴, where an alteration in the hydrogen bonding of Y373 was shown to be responsible for the effect.³² This indicates that the hydrogen bonding network of Y373 is changed in the presence of 8-HDF without disrupting the stabilizing π - π stacking with tryptophane 322. The absorbance peak at 458 nm attributed to 8-HDF was

analyzed by integrating from 450 to 465 nm and fitted monoexponentially (Fig. 3C). For this band a time constant of 1.8 s was determined, only slightly shorter than the values of the TyrO•/FADH• decay constants, implying that the change in the 8-HDF absorption coefficient is linked to the proteins red light-induced formation and decay of the reactive species FADH• and TyrO•.

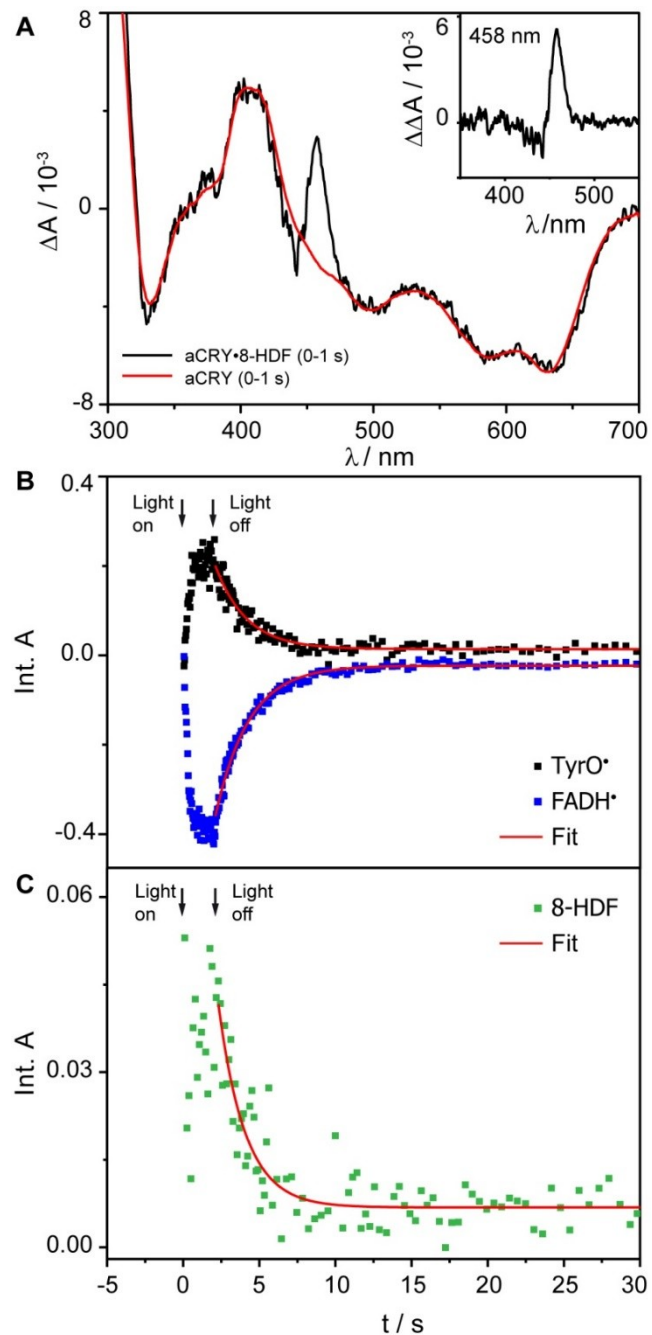
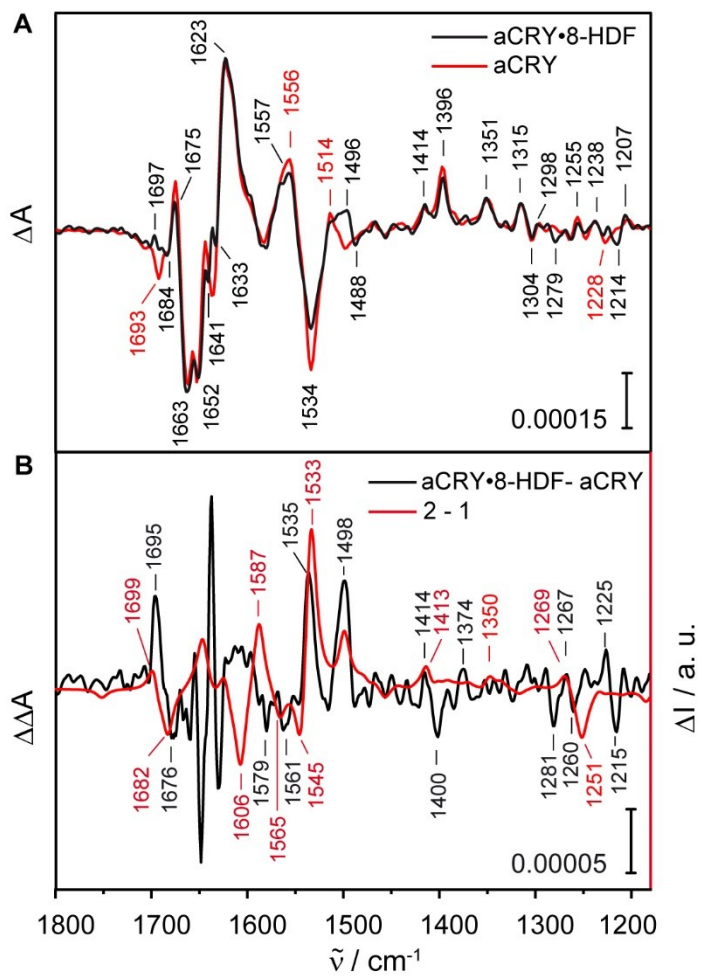


Figure 3. (A) Millisecond time-resolved UV-vis difference spectra of the red light-response in aCRY•8-HDF are compared to aCRY. The samples were illuminated at 632 nm for 2 s to selectively convert FADH• to FADH⁻. The difference spectrum of aCRY•8-HDF shows an additional band at 458 nm assigned to 8-HDF (Inset). (B) The recovery of FADH• and the decay of TyrO• in aCRY•8-HDF were analyzed with monoexponential fits integrating the marker bands at 550-605 nm and 385-425 nm, respectively, both yielding time constants of 2.0 s. (C) The decay of the integrated 8-HDF band from 450-465 nm was fitted monoexponentially yielding a time constant of 1.8 s similar to the TyrO•/FADH⁻ decay.

3.2 FTIR-Spectroscopy. UV-vis spectroscopy of aCRY•8-HDF revealed a transient, red light-induced change in the absorption coefficient of 8-HDF and a shortening of the life-time of TyrO• and FADH⁻ relative to that in aCRY. Red-light-induced FTIR difference spectroscopy in the millisecond time regime was conducted on aCRY•8-HDF and aCRY to investigate the origin of these changes on a structural level. Vibrational modes arising from the presence of 8-HDF in aCRY were analyzed using the rapid-scan technique at 10 °C. Spectra of 4 independent preparations ($\pm 0.11 \cdot 10^{-4} \Delta OD$ at 1557 cm^{-1}) with a time resolution of 70 ms were averaged from 70 ms to 4.1 s and compared to a spectrum of aCRY (9 independent preparations, $\pm 0.25 \cdot 10^{-4} \Delta OD$ at 1557 cm^{-1}) at the same time point taken under identical conditions. Samples were pre-illuminated with blue light for 10 s to form FADH•. After the detection of a reference spectrum FADH⁻ was selectively generated by excitation with red

light for 3 s followed by the immediate start of data acquisition. The light-induced difference spectrum of aCRY•8-HDF at 2 s after illumination shows negative marker bands of FADH• at 1663, 1652 and 1534 cm⁻¹ and positive bands from vibrational modes of FADH⁻ at 1623, 1514, 1351 and 1315 cm⁻¹ in accordance with the aCRY spectrum (Fig 4A) and literature data.^{23, 24} The compliant frequencies of the vibrational modes confirm successful red light-induced generation of FADH⁻ from FADH• in aCRY•8-HDF [\(Supporting information, Tab. S2\)](#).



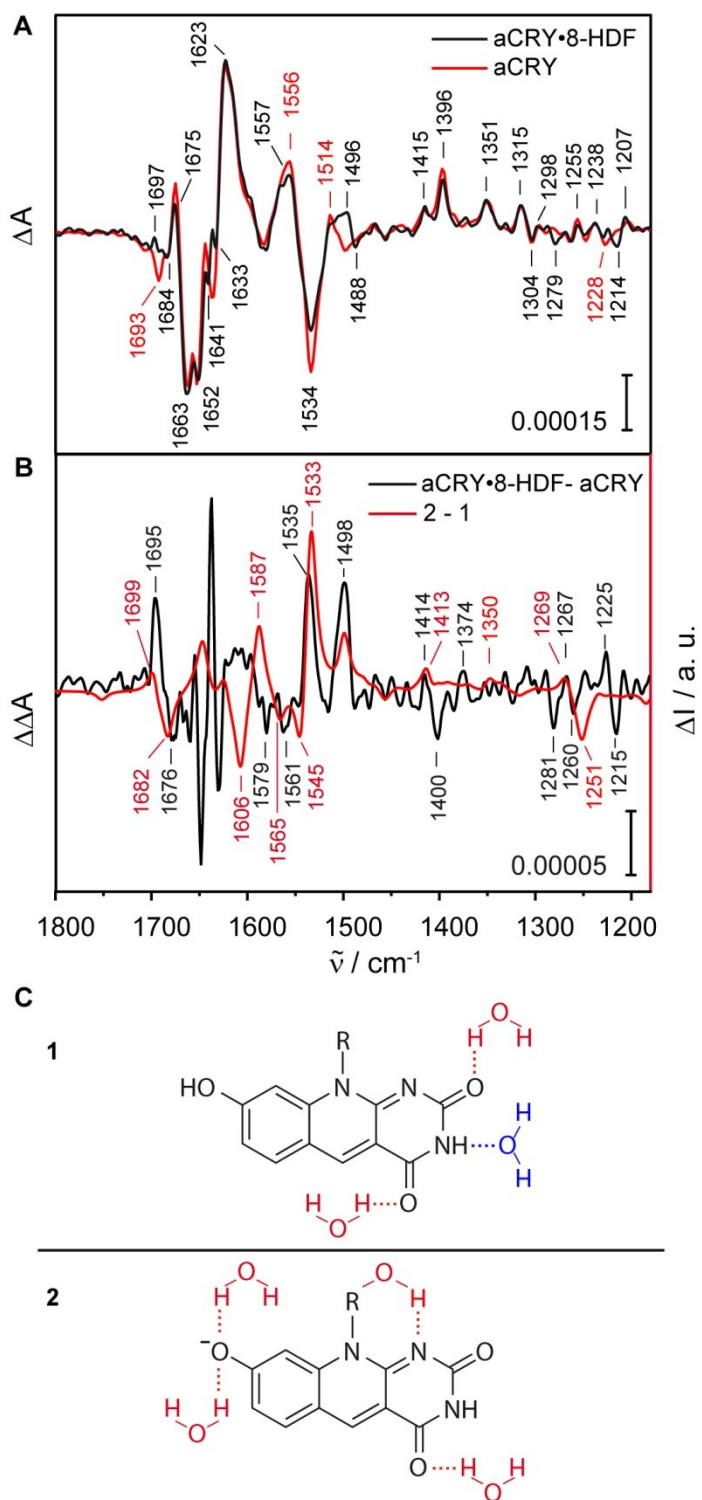


Figure 4. (A) FTIR difference spectra of aCRY•8-HDF and aCRY after red light illumination. The spectra at 2 s of aCRY•8-HDF (black) and aCRY (blue) were

averaged from a continuous series of spectra. The latter was scaled by a factor of 0.51 to the marker band of FADH⁻ at 1351 cm⁻¹. (B) The double difference spectrum of aCRY•8-HDF minus aCRY at 2s (black) is compared to results of the quantum chemical calculations (red). Signals originate from aCRY and model **1** (negative) and aCRY•8-HDF and model **2** (positive). (C) Chemical structures of the 8-HDF models used in the DFT calculations. In model **1** the 8-hydroxyl group of 8-HDF is protonated, representing the chromophore in the dark state. Model **2** shows the deprotonated 8-hydroxyl group as the acceptor of two hydrogen bonds as assigned to the state after red light-illumination.

3.2.1 Red light-induced changes in the 8-HDF protonation state.

Vibrational modes arising from the presence of 8-HDF in aCRY were isolated by calculating the double difference spectrum of the aCRY•8-HDF minus the aCRY spectrum after scaling the latter to the marker band of FADH⁻ at 1351 cm⁻¹ by a factor of 0.51 (Fig. 4B). The correct scaling was confirmed by the consistent intensity of multiple positive and negative flavin bands at 1315, 1304, and 1298 cm⁻¹ (Fig. 4A). DFT calculations of 8-HDF with different protonation states and hydrogen bonding scenarios at the oxygen of the 8-hydroxyl and the carbonyl and amine groups were performed and used for band assignment due to very good agreement of calculated and experimentally obtained spectra in previous studies.^{23, 32, 48-50} The difference spectrum of the deprotonated 8-HDF accepting two hydrogen bonds from two water molecules at the 8-hydroxyl group and each a hydrogen bond at

the 1-amine and 4-carbonyl group, model 2, minus the protonated 8-HDF accepting a hydrogen bond at the 2- and 4-carbonyl group and donating one at the 3-amine group, model 1, (Fig. 4C) yielded the best agreement with the experimental data ~~and were used for the band assignment~~ (Fig. 4B). Based on the calculations, a simple change of the hydrogen bond pattern at the 8-hydroxyl group as the origin for the observed bands could be ruled out (Fig. S4). The assignments were supported by calculating potential energy distributions (Supporting [Material information](#), Tables [S2-S3](#) and [S3S4](#)). In the calculated spectra, the relative intensities of the bands of are not fully representative. The double difference bands from 1660-1580 cm^{-1} were omitted in the analysis because of the strong absorption of water in this region.

The negative bands in the experimental spectrum (Fig. 4B) originate either from modes of the protonated 8-HDF or the protein matrix exhibiting smaller or negative intensity in the aCRY•8-HDF difference spectrum as compared to aCRY. For clarity, the following section will discuss only bands attributed to 8-HDF. An assignment of the remaining bands can be found in the supporting information (Tab. [S4S5](#)).

In the experimental spectrum a negative band at 1676 cm^{-1} is present, assignable to the CO stretching vibration of the 8-HDF 2-carbonyl group found at 1682 cm^{-1} in the calculated spectrum. The two negative bands at 1579 and 1561 cm^{-1} can be assigned to the CC ring and the CN ring stretching mode of the antenna chromophore, respectively. The calculated

spectrum also exhibits these features, slightly downshifted at 1565 and 1545 cm^{-1} , respectively. In the protein spectrum, a mode at 1260 cm^{-1} is present, assignable to the 8-hydroxyl CO stretching vibration found at 1251 cm^{-1} in the calculated difference spectrum.

Positive bands in the double difference spectrum arise from either 8-HDF in the deprotonated state or bands with a higher intensity in the aCRY•8-HDF spectrum originating from the protein matrix. The most prominent positive double difference bands in the experimental data are found at 1535 and 1498 cm^{-1} and are not assignable to the flavin chromophore or amino acid residues. Although the band at 1535 cm^{-1} is still found within the amid II region, this band is assigned to 8-HDF as in the calculated spectrum a vibrational mode at a similar frequency of 1533 cm^{-1} originating from the CN ring stretching mode and the CO stretching vibration of the deprotonated 8-hydroxyl group is present. The band at 1498 cm^{-1} can unambiguously be assigned to the deprotonated 8-HDF as a mode at the identical position is found in the calculated spectrum, with main contributions from the CO stretching of the 8-hydroxyl group and the CC ring stretching vibration.

The band at 1414 cm^{-1} can be assigned to the CC stretching mode of the 8-HDF ring system, in agreement with the DFT calculations where the band is found at 1413 cm^{-1} . At 1267 cm^{-1} a small positive mode arises from a CHH bending mode of the ribityl chain as confirmed by a band at 1269 cm^{-1} in the calculated spectrum.

Table 1. Vibrational frequencies of 8-HDF contributions in the aCRY•8-HDF *minus* aCRY spectrum compared to the calculated difference spectrum for model 2 *minus* 1. The frequencies are given in cm⁻¹.

aCRY•8-HDF- aCRY		Calculati on	Assignment
Positiv e	Negativ e		
	1676	1682	8-HDF ν_{C_2O} ^a
	1579	1565	8-HDF ν_{CC} ring , δ_{C_8OH} _b ,
	1561	1545	8-HDF $\nu_{CN_{ring}}$
1535		1533	8-HDF ⁻ $\nu_{CN_{ring}}$, ν_{C_8O}
1498		1498	8-HDF ⁻ $\nu_{CC_{ring}}$, ν_{C_8O}
1414		1413	8-HDF ⁻ $\nu_{CC_{ring}}$
1267		1269	8-HDF ⁻ $\delta_{CHH_{ribity\ chain}}$
	1260	1251	8-HDF ν_{C_8O}

FADH⁻ formation^{23, 51}, this band is assigned to alterations of the hydrogen bonding network of N395 in the presence of 8-HDF.

This finding supports the suggestion that the amino acid plays a key role in the stabilization of FADH[•] in aCRY•8-HDF by acting as a gate keeper for a proton transferred from a water molecule. Only a small shoulder at 1684 cm⁻¹ represents the negative counterpart in the double difference spectrum due to the overlay of the negative band at 1684 cm⁻¹ in the aCRY•8-HDF spectrum with the positive band in the aCRY spectrum at 1686 cm⁻¹ (Figure 4A).

3.5 Characteristics of aCRY•8-HDF fluorescence emission in dependence of the flavin oxidation state. Fluorescence spectra of aCRY•8-HDF carrying FAD_{ox} were compared to aCRY with FAD_{ox}, deprotonated 8-HDF in a phosphate buffer and DMSO each with 0.1% Et₃N (Fig. 5A). The fluorescence spectrum of aCRY•8-HDF carrying FAD_{ox} shows a maximum at 459 nm and a shoulder at 489 nm distinctly blue shifted compared to the spectrum of aCRY with maxima at 492 and 530 nm. Interestingly, the comparison of the fluorescence intensity of both samples reveals a tenfold higher intensity of the aCRY•8-HDF emission as compared to aCRY. The very weak fluorescence of aCRY with FAD_{ox} (blue curve, Fig. 5A) can be explained by the quenching of flavin via ultrafast electron transfer from a neighboring tryptophan.⁵² Consequently, the stronger fluorescence and the spectral shift in the aCRY•8-HDF emission spectrum relative to aCRY indicates a predominant fluorescence contribution from 8-HDF.

The spectra of the deprotonated 8-HDF in phosphate buffer and DMSO with each 0.1% Et₃N show red-shifted emission maxima at 465 and 474 nm, respectively, presumably as a result of rapid solvation dynamics. To compare the fluorescence yield of aCRY•8-HDF to 8-HDF in phosphate buffer with 0.1% Et₃N the samples were adjusted to the same 8-HDF concentration. The fluorescence intensity of the antenna chromophore in buffer was found to be 13 times higher as compared to aCRY•8-HDF with FAD_{ox} (data not shown), implying the quenching of the 8-HDF fluorescence by a resonant energy transfer to flavin as observed before in photolyases.^{34, 36, 53}

Additionally, the fluorescence of aCRY•8-HDF was investigated as a function of the flavin oxidation state. FADH• was generated upon 10 s of blue light illumination and a permanent stabilization of FADH⁻ was achieved upon addition of 10 μM ascorbic acid and 40 s of blue light illumination (Fig. 5B). Upon the conversion of FAD_{ox} to FADH• in aCRY•8-HDF the fluorescence intensity doubled without a change in the band shape (Fig 5B, inset). In the dark, the fluorescence intensity decreased over time (Fig. S21). After conversion from FADH• to FADH⁻ the fluorescence emission of aCRY•8-HDF increased in intensity by 20% and showed a slight increase in the shoulder at 489 nm, indicating a contribution from free flavin due to release upon intense illumination in the presence of ascorbic acid (Fig. S53).

The theoretical RET efficiencies for 8-HDF to FAD_{ox}, FADH• and FADH⁻ were calculated to be 99.6%, 99.7% and 97.0%, respectively. Noticeably, the efficiencies for FAD_{ox} and FADH• are almost identical, not explaining the

experimentally observed increase in fluorescence emission upon FADH• formation. The transfer efficiency calculated for FADH⁻ is lower than for FAD_{ox} and FADH•, as expected due to the smaller overlap integral and is thus in agreement with the rise in intensity observed in the emission spectra.

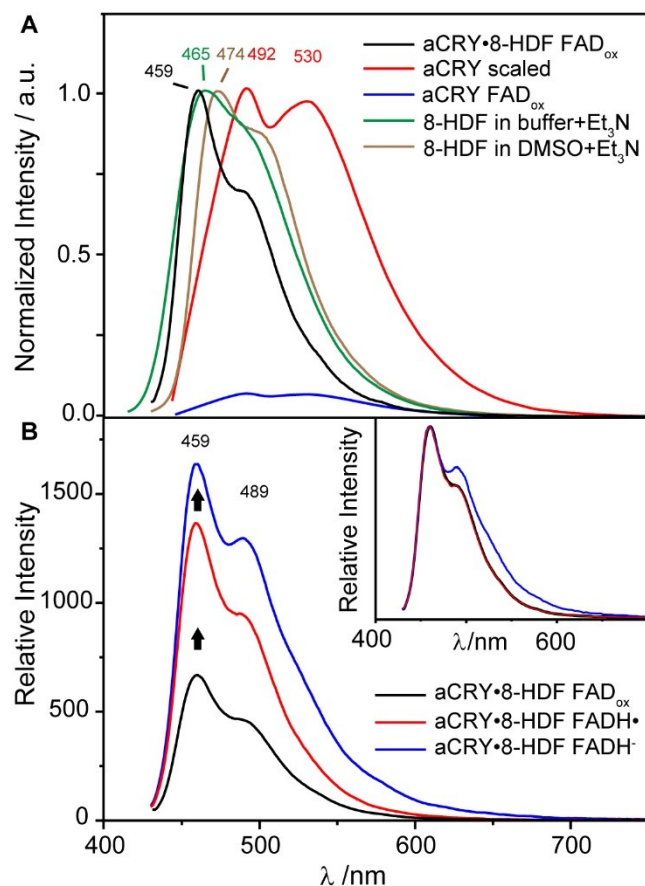


Figure 5. (A) Spectra of aCRY•8-HDF carrying FAD_{ox} are compared to spectra of aCRY with FAD_{ox}, 8-HDF in DMSO+0.1% Et₃N and in phosphate buffer+0.1% Et₃N. All data sets are scaled to the emission maximum of aCRY•8-HDF except for the spectra of aCRY with FAD_{ox} (blue). The spectrum of aCRY•8-HDF shows distinct emission bands at 459 and 489 nm blue shifted compared to aCRY with maxima at 492 and 530 nm. (B) Fluorescence

spectra of aCRY•8-HDF carrying either FAD_{ox}, FADH• or FADH⁻. FAD_{ox} in aCRY•8-HDF (black) was converted to FADH• (red) by blue light illumination for 10 s resulting in a doubling of the fluorescence intensity with no change in band shape (Inset). The reduction of FADH• to FADH⁻ by 40 s blue light illumination in the presence of ascorbic acid induces an additional intensity surge of ~20%.

4. DISCUSSION

4.1 Stabilization of FADH• by the presence of 8-HDF. Previous work shows that aCRY carries the flavin neutral radical in the dark state of the receptor *in vivo*²⁰, although it was found to decay rapidly *in vitro*.²³ In order to elucidate the impact of the binding of 8-HDF on the stability of FADH•, its decay was monitored over a time course of several hours (Fig. 2B), revealing an increase in the major component of the lifetime ~~major component~~ in aCRY•8-HDF by a factor of 3.5. As the decay of FADH• was shown to be pH dependent²³, it was suggested that the deprotonation kinetics is controlled either directly by a neighboring amino acid such as a histidine or indirectly by asparagine 395 functioning as a gate keeper for a proton transferred from the solvent.^{23, 29} Evidence for the latter hypothesis is found in the FTIR double difference spectra of aCRY•8-HDF *minus* aCRY (Fig. 4B), showing a prominent positive band at 1695 cm⁻¹ close to a position previously assigned to red light-induced changes in the hydrogen bonding of N395.²³ It can be concluded that the presence of 8-HDF alters the hydrogen bonding network

in the flavin binding pocket, which manifests itself in the stabilization of FADH• and decreasing life-time of FADH• from 2.6 to 2.0 ms as observed in the UV-vis data (Fig. 2B and Fig. 3B). This finding is quite unusual, given the chromophores distance of 17.4 Å and the lack of obvious structural deviations in the flavin binding pocket in the crystal structures of aCRY and aCRY•8-HDF.²⁹ Interestingly, in the 8-HDF binding pocket the phenylalanine 43 (F43) flips upon binding in the presence of 8-HDF to form a π - π stacking with the antenna.²⁹ This rearrangement could induce alterations in the hydrogen bonding network of the entire protein spanning wide enough to alter the hydrogen bonding network in the flavin binding pocket. Due to the lack of structural rearrangements in the binding pocket on a larger scale, it seems unlikely that the redox potential of the neutral radical is modulated in presence of 8-HDF, ruling this effect out as a cause for the longer lifetime of FADH•. Nevertheless, it has to be tested in future experiments if the stability of FADH• in aCRY•8-HDF is also irresponsive to changing oxygen levels as observed previously in aCRY only carrying flavin.²³

From a physiological point of view, the extended life time of the neutral radical in presence of 8-HDF explains how aCRY can fulfill its function as a red light receptor *in vivo* since FADH• is the only flavin oxidation state with an expanded spectral sensitivity up to 680 nm. The ability to sense red light is essential for photosynthetic organisms in order to control adaptive process for example in response to low light conditions and generally enables the organism to detect not only varying light quantities but also qualities. As no

[phytochrome or other red light receptor was identified in *C. reinhardtii* to date⁵⁴, the role of aCRY as a red light receptor is even more important in the green alga.](#)

4.2 Red light-induced deprotonation of 8-HDF. Millisecond time-resolved UV-vis experiments show an additional absorbance band at 458 nm in the aCRY•8-HDF spectrum, decaying concomitantly with the reactive species TyrO• and FADH•. The band at 458 nm is assigned to the red light-induced bathochromic shift in the 8-HDF absorption [by 10 nm](#) (Fig. 3A). [A similar but even more pronounced red shift is observed upon the deprotonation of 8-HDF in solution, where the neutral form absorbs at 390 nm and the anion has a maximum at 421 nm^{33, 55}, indicating the deprotonation of 8-HDF in aCRY•8-HDF upon flavin reduction. Although the absorption maximum of neutral 8-HDF is found at 390 nm, 60 nm blue shifted compared to the protein bound 8-HDF, in the F420-binding protein of *M. tuberculosis* the neutral form of 8-HDF shows an absorbance maximum at 440 nm⁵⁶, revealing the strong impact of the protein environment on position of the absorbance maximum and supporting the presence of neutral 8-HDF in aCRY•8-HDF.](#) Previously, the strong red shift of the 8-HDF absorbance in photolyases as compared to solution was attributed to a negative solvatochromism as expected for charged species⁵⁷ such as the ~~deprotonated 8-HDF anion induced by in the~~ a non-polar environment ~~of 8-HDF~~ in these proteins^{12, 35}. Compared to other photolyases carrying 8-HDF, in aCRY•8-HDF the absorption shift is especially pronounced with a maximum

found at 448 nm^{29, 36}. Only the (6-4) photolyase of *D. melanogaster* shows an equal shift to the red^{10, 36} implying that both 8-HDF binding pockets harbor similar nonpolar amino acids. However, in aCRY•8-HDF, F43 forms a π - π stacking with 8-HDF representing a logical cause for the red shift, whereas the corresponding amino acid in (6-4) *D. melanogaster* is isoleucine 50. Furthermore, in the *M. mazei* CPD photolyase the phenylalanine 61 is also found in a π - π stacking without causing the red shift, shown by the absorbance maximum at (A_{\max} =435 nm).³⁶ Interestingly, in this protein the exchange of the polar serine 26 to the nonpolar leucine induced a blue shift of the absorbance to 432 nm. Contrary to conventional thought, this hints towards a positive solvatochromism of 8-HDF in the photolyase and leaves questions about its actual protonation state. The respective amino acid at this position sensitive to changes in the polarity in aCRY•8-HDF and the *D. melanogaster* (6-4) photolyase is a negatively positively charged arginine (R12 and R13, respectively). This supports the theory of a positive solvatochromic effect, attributing supporting the assignment of the observed red-shift in the 8-HDF absorption to the formation of a charged species such as the 8-HDF anion.

This theory is supported by the comparison of the FTIR data with DFT calculations of 8-HDF at different protonation states, which allowed the assignment of the bands at 1535 and 1498 cm^{-1} to the CO stretching vibration of the 8-HDF anion. For the modeling of the negative bands of the experimental data, a calculated spectrum of the protonated 8-HDF gave the

best results. Here, the COH bending vibration of the hydroxyl group and a CN ring stretching mode, found at 1565 cm^{-1} and 1545 cm^{-1} , respectively, are slightly downshifted compared to the bands from the experimental data found at 1579 and 1561 cm^{-1} . The down shift can be attributed to the complex environment of the hydroxyl group in the antenna binding pocket which might not be completely mimicked in the calculations. In the two models also the hydrogen bonding structure of the carbonyl and amine groups of 8-HDF differ, indicating overall changes in the hydrogen bonding network in the antenna binding pocket. Finally, the very good agreement of the calculated difference spectrum of the deprotonated 8-HDF⁻ minus the protonated 8-HDF with the experimental data supports the theory of the red light-induced deprotonation of the antenna, indicating a long range coupling of the chromophores via the hydrogen bonding network.

4.3 Energy transfer processes in aCRY•8-HDF in dependence of the flavin oxidation state. To date, energy transfer processes in cryptochromes have not been studied extensively. Here, we investigated this phenomenon in a cryptochrome carrying FAD and 8-HDF. The fluorescence emission spectrum of aCRY•8-HDF shows a 13 times lower intensity than 8-HDF solvated in phosphate buffer, resulting from the quenching via RET between flavin and 8-HDF in aCRY•8-HDF as observed previously in photolyases^{34, 53} and the *Vibrio cholera* cryptochrome VcCry1 between FAD and MTHF.⁵⁸

Remarkably, a doubling of fluorescence yield occurred upon the light-induced conversion from FAD_{ox} to FADH^\bullet , followed by an additional intensity surge upon FADH^- formation (Fig. 5B). Interestingly, only for the conversion from FADH^\bullet to FADH^- a similar phenomenon was reported for *A. nidulans* (6-4) and *E. coli* photolyases.^{34, 53, 59} The observed intensity surge upon FADH^- formation is not completely in agreement with the results of the efficiency calculations, where a difference of around 4% is predicted opposed to 20% in our experimental spectra. The difference might be explained by the release of flavin upon FADH^- generation given the RET efficiency of 97.0% for FADH^- being in a similar range of previously determined transfer efficiencies of other photolyases of 99.6% and 92%.^{45, 53} While the increase of fluorescence emission upon FADH^- formation can be rationalized by the smaller overlap integral, J , between 8-HDF and FADH^- as compared to FADH^\bullet , the increase observed upon conversion from FAD_{ox} to FADH^\bullet is not reflected by the calculations and has not been observed before. On a molecular level, changes in the orientation factor κ^2 upon 8-HDF deprotonation and flavin reduction might be responsible for this phenomenon. In the *E. coli* photolyase, it was shown that the reduction of FAD_{ox} to FADH^\bullet and FADH^- led to significant changes in κ^2 caused by alterations in the transition dipole moment.⁵⁹ Considering that 8-HDF might be partially deprotonated upon FADH^\bullet formation, the transition dipole moment of 8-HDF will also change. In that case, κ^2 might be altered even more drastically, resulting in changes in RET efficiencies. In order to verify this theory, time-dependent density

functional theory for the determination of the transition dipole moments could be employed.

Even upon FADH⁻ formation, the fluorescence intensity of solvated 8-HDF is still 6-times higher. Nevertheless, in aCRY•8-HDF the fluorescence intensity is not as strongly reduced as in 8-HDF binding photolyases such as the *A. nidulans* (6-4) photolyase, where a 25-fold decrease is observed^{34, 60}, indicating a less efficient energy transfer between 8-HDF and FADH⁻ in aCRY•8-HDF. Due to an additional purification step of the samples prior to the experiments the contribution from free chromophore as a source for the higher intensity can be ruled out. Since aCRY•8-HDF has a dual function as a red-light receptor as well as a (6-4) photolyase, the reduced energy transfer efficiency might help to keep the balance between over excitation when acting as a red-light receptor and DNA repair efficiency when acting as a photolyase. The change of the transfer efficiency in dependence of the flavin oxidation state could be used by the protein to further regulate the amount of light energy needed for the respective task. Picosecond transient absorption spectroscopy might help to reveal the dissipation pathways of the transferred light energy

5. CONCLUSIONS

In this study, the essential role of the antenna pigment 8-HDF for the functionality of the bifunctional cryptochrome aCRY beyond the sole purpose of light harvesting is disclosed. The binding of 8-HDF at a 17.4 Å distance to the flavin significantly stabilizes the dark state of the receptor, FADH•, *in*

vitro. Changes in the hydrogen bonding network of N395 in the flavin binding pocket are responsible for the effect as evidenced by FTIR spectroscopy. Upon red-light excitation of FADH•, 8-HDF shows a red-shift in UV-vis absorption concomitant to the formation and decay of the reactive species, FADH• and TyrO•. Based on the presented FTIR spectra and quantum chemical calculations we propose the changes to originate from the deprotonation of 8-HDF upon FADH• formation, questioning the paradigm of 8-HDF as being permanently bound in its deprotonated state in cryptochromes and photolyases. Investigation of the energy transfer processes revealed a drastic decrease in transfer efficiency of 8-HDF upon flavin reduction, likely linked to the deprotonation of 8-HDF, a phenomenon not observed before and possibly responsible for the balancing of aCRYs dual function.

Here, the interdependence of an antenna pigment and a light-sensing chromophore via a long range hydrogen bonding network is presented and supported by experimental and theoretical data. In aCRY•8-HDF this coupling is found to be essential for the protein's function as a red light receptor and we suggest this connection to also regulate the energy transfer efficiency from 8-HDF to flavin. This represents an effective mechanism to control the activation of aCRY and possibly facilitate the dual function as both photolyase and red-light receptor. Since several bifunctional cryptochromes are known to date⁶¹⁻⁶⁵, this concept represents a plausible strategy also employed by other members in this protein family.

ASSOCIATED CONTENT

Accession Code: A8J8W0

Supporting Information. Supplementary Text: [Material and Methods: Size exclusion chromoptography](#), Assignment and discussion of vibrational modes arising from changes in the hydrogen bonding network of tyrosine 373. Experimental Data: [S1: Absorbance spectra of aCRY8-HDF after size exclusion chromatography](#), [S21: Fluorescence emission spectra](#), [S3: Alternative chemical structures and DFT calculations](#), [S42: Overlap integral used to calculate the Foerster efficiency](#), [S53: Difference spectrum of the scaled fluorescence emission of aCRY•8-HDF](#), [S64: Optimized structure of the deprotonated 8-hydroxy-5-deazaflavin](#), Table S1: Parameters used to calculate the Foerster resonance energy transfer efficiencies, [Table S2: Assignment of the FT-IR difference bands of aCRY•8-HDF and aCRY after the conversion of FADH• to FADH⁻](#), Table S32: PED Analysis 8-HDF. Table S43: PED Analysis 8-HDF anion; Table S54: Assignment of vibrational modes originating from the residues asparagine 395 and tyrosine 373. This material is available free of charge via the Internet at <http://pubs.acs.org>.

AUTHOR INFORMATION

Corresponding Author

*Sabine Oldemeyer: soldemeyer@lbl.gov

Author Contributions

S.O. designed the study. S. O. performed and analyzed the experiments with advice by G. F. and A. H.. S. O. wrote the manuscript with advice by A. H. and G. F.. All authors have given approval to the final version of the manuscript.

Funding Sources

This work was supported by the Deutsche Forschungsgemeinschaft (DFG) with the DFG grant OI555/1-1 to S.O. The quantum chemical calculations were performed with the support of NIH S10OD023532. A.Z.H. was supported by the Department of Energy Solar Energy Technologies Office, award number DE-EE00032324. G.R.F. was supported by the US Department of Energy, Office of Science, Basic Energy Sciences, Chemical Sciences, Geosciences, and Biosciences Division.

Notes

The authors declare no competing financial interest.

ACKNOWLEDGMENT

We thank Tilman Kottke and Christian Thöing for their support. We thank Jens Christoffers for providing synthetic 8-HDF.

ABBREVIATIONS

8-HDF, 8-hydroxy-5-deazaflavin; CraCRY, *Chlamydomonas reinhardtii* animal-like cryptochrome; DFT, density functional theory; DMLR, 6,7-dimethyl-8-ribityllumazine; FAD, Flavin adenine dinucleotide; FADH•, Flavin neutral radical; FADH⁻, Flavin fully reduced state; FTIR, Fourier transform infrared;

FMN, flavin mononucleotide; MTHF: 5,10-methenyltetrahydrofolate; PHR, photolyase homology region.

REFERENCES

- (1) Sancar, A. (2003) Structure and function of DNA photolyase and cryptochrome blue-light photoreceptors, *Chem. Rev.* **103**, 2203-2237.
- (2) Losi, A., and Gärtner, W. (2012) The evolution of flavin-binding photoreceptors: an ancient chromophore serving trendy blue-light sensors, *Annu. Rev. Plant Biol.* **63**, 49-72.
- (3) Chaves, I., Pokorny, R., Byrdin, M., Hoang, N., Ritz, T., Brettel, K., Essen, L. O., van der Horst, G. T., Batschauer, A., and Ahmad, M. (2011) The cryptochromes: blue light photoreceptors in plants and animals, *Annu. Rev. Plant Biol.* **62**, 335-364.
- (4) Lin, C., and Shalitin, D. (2003) Cryptochrome structure and signal transduction, *Annu. Rev. Plant Biol.* **54**, 469-496.
- (5) Hore, P. J., and Mouritsen, H. (2016) The Radical-Pair Mechanism of Magnetoreception, *Annual Review of Biophysics* **45**, 299-344.
- (6) Rupert, C. S. (1960) Photoreactivation of transforming DNA by an enzyme from bakers' yeast, *J. Gen. Physiol* **43**, 573-595.
- (7) Todo, T., Takemori, H., Ryo, H., Ihara, M., Matsunaga, T., Nikaido, O., Sato, K., and Nomura, T. (1993) A new photoreactivating enzyme that specifically repairs ultraviolet light-induced (6-4) photoproducts, *Nature* **361**, 371-374.
- (8) Johnson, J. L., Hamm-Alvarez, S., Payne, G., Sancar, G. B., Rajagopalan, K. V., and Sancar, A. (1988) Identification of the second chromophore of *Escherichia coli* and yeast DNA photolyases as 5,10-methenyltetrahydrofolate, *Proc. Natl. Acad. Sci. U. S. A.* **85**, 2046-2050.
- (9) Klar, T., Pokorny, R., Moldt, J., Batschauer, A., and Essen, L. O. (2007) Cryptochrome 3 from *Arabidopsis thaliana*: structural and functional analysis of its complex with a folate light antenna, *J. Mol. Biol.* **366**, 954-964.
- (10) Glas, A. F., Maul, M. J., Cryle, M., Barends, T. R., Schneider, S., Kaya, E., Schlichting, I., and Carell, T. (2009) The archaeal cofactor F0 is a light-harvesting antenna chromophore in eukaryotes, *Proc. Natl. Acad. Sci. U. S. A.* **106**, 11540-11545.
- (11) Selby, C. P., and Sancar, A. (2012) The second chromophore in *Drosophila* photolyase/cryptochrome family photoreceptors, *Biochemistry* **51**, 167-171.
- (12) Eker, A. P., Kooiman, P., Hessels, J. K., and Yasui, A. (1990) DNA photoreactivating enzyme from the cyanobacterium *Anacystis nidulans*, *Journal of Biological Chemistry* **265**, 8009-8015.
- (13) Ueda, T., Kato, A., Kuramitsu, S., Terasawa, H., and Shimada, I. (2005) Identification and characterization of a second chromophore of DNA

- photolyase from *Thermus thermophilus* HB27, *J. Biol. Chem.* 280, 36237-36243.
- (14) Geisselbrecht, Y., Frühwirth, S., Schroeder, C., Pierik, A. J., Klug, G., and Essen, L. O. (2012) CryB from *Rhodobacter sphaeroides*: a unique class of cryptochromes with new cofactors, *EMBO Rep.* 13, 223-229.
- (15) Fujihashi, M., Numoto, N., Kobayashi, Y., Mizushima, A., Tsujimura, M., Nakamura, A., Kawarabayasi, Y., and Miki, K. (2007) Crystal structure of archaeal photolyase from *Sulfolobus tokodaii* with two FAD molecules: implication of a novel light-harvesting cofactor, *J. Mol. Biol.* 365, 903-910.
- (16) Yang, H. Q., Wu, Y. J., Tang, R. H., Liu, D., Liu, Y., and Cashmore, A. R. (2000) The C termini of *Arabidopsis* cryptochromes mediate a constitutive light response, *Cell* 103, 815-827.
- (17) Kutta, R. J., Archipowa, N., and Scrutton, N. S. (2018) The sacrificial inactivation of the blue-light photosensor cryptochrome from *Drosophila melanogaster*, *Phys Chem Chem Phys* 20, 28767-28776.
- (18) Kottke, T., Oldemeyer, S., Wenzel, S., Zou, Y., and Mittag, M. (2017) Cryptochrome photoreceptors in green algae: Unexpected versatility of mechanisms and functions, *Journal of Plant Physiology* 217, 4-14.
- (19) Fortunato, A. E., Annunziata, R., Jaubert, M., Bouly, J. P., and Falciatore, A. (2015) Dealing with light: The widespread and multitasking cryptochrome/photolyase family in photosynthetic organisms, *J. Plant Physiol.* 172C, 42-54.
- (20) Beel, B., Prager, K., Spexard, M., Sasso, S., Weiss, D., Müller, N., Heinnickel, M., Dewez, D., Ikoma, D., Grossman, A. R., Kottke, T., and Mittag, M. (2012) A Flavin Binding Cryptochrome Photoreceptor Responds to Both Blue and Red Light in *Chlamydomonas reinhardtii*, *Plant Cell* 24, 2992-3008.
- (21) Bouly, J. P., Schleicher, E., Dionisio-Sese, M., Vandenbussche, F., Van Der Straeten, D., Bakrim, N., Meier, S., Batschauer, A., Galland, P., Bittl, R., and Ahmad, M. (2007) Cryptochrome blue light photoreceptors are activated through interconversion of flavin redox states, *J. Biol. Chem.* 282, 9383-9391.
- (22) Banerjee, R., Schleicher, E., Meier, S., Viana, R. M., Pokorny, R., Ahmad, M., Bittl, R., and Batschauer, A. (2007) The signaling state of *Arabidopsis* cryptochrome 2 contains flavin semiquinone, *J. Biol. Chem.* 282, 14916-14922.
- (23) Spexard, M., Thöing, C., Beel, B., Mittag, M., and Kottke, T. (2014) Response of the Sensory Animal-like Cryptochrome aCRY to Blue and Red Light As Revealed by Infrared Difference Spectroscopy, *Biochemistry* 53, 1041-1050.
- (24) Oldemeyer, S., Franz, S., Wenzel, S., Essen, L. O., Mittag, M., and Kottke, T. (2016) Essential Role of an Unusually Long-lived Tyrosyl Radical in the Response to Red Light of the Animal-like Cryptochrome aCRY, *J. Biol. Chem.* 291, 14062-14071.

- (25) Franz-Badur, S., Penner, A., Straß, S., von Horsten, S., Linne, U., and Essen, L.-O. (2019) Structural changes within the bifunctional cryptochrome/photolyase CraCRY upon blue light excitation, *Sci Rep* 9, 9896-9896.
- (26) Berndt, A., Kottke, T., Breitzkreuz, H., Dvorsky, R., Hennig, S., Alexander, M., and Wolf, E. (2007) A novel photoreaction mechanism for the circadian blue light photoreceptor *Drosophila* cryptochrome, *J. Biol. Chem.* 282, 13011-13021.
- (27) Immeln, D., Schlesinger, R., Heberle, J., and Kottke, T. (2007) Blue light induces radical formation and autophosphorylation in the light-sensitive domain of *Chlamydomonas* cryptochrome, *J. Biol. Chem.* 282, 21720-21728.
- (28) Müller, P., and Ahmad, M. (2011) Light-activated Cryptochrome Reacts with Molecular Oxygen to Form a Flavin-Superoxide Radical Pair Consistent with Magnetoreception, *J. Biol. Chem.* 286, 21033-21040.
- (29) Franz, S., Ignatz, E., Wenzel, S., Zielosko, H., Putu, E. P. G. N., Maestre-Reyna, M., Tsai, M.-D., Yamamoto, J., Mittag, M., and Essen, L.-O. (2018) Structure of the bifunctional cryptochrome aCRY from *Chlamydomonas reinhardtii*, *Nucleic Acids Res* 46, 8010-8022.
- (30) Lacombat, F., Espagne, A., Dozova, N., Plaza, P., Müller, P., Brettel, K., Franz-Badur, S., and Essen, L.-O. (2019) Ultrafast Oxidation of a Tyrosine by Proton-Coupled Electron Transfer Promotes Light Activation of an Animal-like Cryptochrome, *Journal of the American Chemical Society* 141, 13394-13409.
- (31) Nohr, D., Franz, S., Rodriguez, R., Paulus, B., Essen, L. O., Weber, S., and Schleicher, E. (2016) Extended Electron-Transfer in Animal Cryptochromes Mediated by a Tetrad of Aromatic Amino Acids, *Biophys. J.* 111, 301-311.
- (32) Oldemeyer, S., Mittag, M., and Kottke, T. (2019) Time-Resolved Infrared and Visible Spectroscopy on Cryptochrome aCRY: Basis for Red Light Reception, *Biophysical Journal* 117, 490-499.
- (33) Eirich, L. D., Vogels, G. D., and Wolfe, R. S. (1979) Distribution of coenzyme F420 and properties of its hydrolytic fragments, *J Bacteriol* 140, 20-27.
- (34) Malhotra, K., Kim, S. T., Walsh, C., and Sancar, A. (1992) Roles of FAD and 8-hydroxy-5-deazaflavin chromophores in photoreactivation by *Anacystis nidulans* DNA photolyase, *Journal of Biological Chemistry* 267, 15406-15411.
- (35) Jacobson, F., and Walsh, C. (1984) Properties of 7,8-didemethyl-8-hydroxy-5-deazaflavins relevant to redox coenzyme function in methanogen metabolism, *Biochemistry* 23, 979-988.
- (36) Kiontke, S., Gnau, P., Haselsberger, R., Batschauer, A., and Essen, L. O. (2014) Structural and Evolutionary Aspects of Antenna Chromophore Usage by Class II Photolyases, *J. Biol. Chem.* 289, 19659-19669.
- (37) Swinehart, D. F. (1962) The Beer-Lambert Law, *Journal of Chemical Education* 39, 333.

- (38) Siegel, L. M. (1978) Quantitative determination of noncovalently bound flavins: types and methods of analysis, *Methods Enzymol.* 53, 419-429.
- (39) Artimo, P., Jonnalagedda, M., Arnold, K., Baratin, D., Csardi, G., de Castro, E., Duvaud, S., Flegel, V., Fortier, A., Gasteiger, E., Grosdidier, A., Hernandez, C., Ioannidis, V., Kuznetsov, D., Liechti, R., Moretti, S., Mostaguir, K., Redaschi, N., Rossier, G., Xenarios, I., and Stockinger, H. (2012) ExpASY: SIB bioinformatics resource portal, *Nucleic Acids Res.* 40, W597-603.
- (40) Frisch, M. J., Trucks, G. W., Schlegel, H. B., Scuseria, G. E., Robb, M. A., Cheeseman, J. R., Scalmani, G., Barone, V., Petersson, G. A., Nakatsuji, H., Li, X., Caricato, M., Marenich, A. V., Bloino, J., Janesko, B. G., Gomperts, R., Mennucci, B., Hratchian, H. P., Ortiz, J. V., Izmaylov, A. F., Sonnenberg, J. L., Williams, Ding, F., Lipparini, F., Egidi, F., Goings, J., Peng, B., Petrone, A., Henderson, T., Ranasinghe, D., Zakrzewski, V. G., Gao, J., Rega, N., Zheng, G., Liang, W., Hada, M., Ehara, M., Toyota, K., Fukuda, R., Hasegawa, J., Ishida, M., Nakajima, T., Honda, Y., Kitao, O., Nakai, H., Vreven, T., Throssell, K., Montgomery Jr., J. A., Peralta, J. E., Ogliaro, F., Bearpark, M. J., Heyd, J. J., Brothers, E. N., Kudin, K. N., Staroverov, V. N., Keith, T. A., Kobayashi, R., Normand, J., Raghavachari, K., Rendell, A. P., Burant, J. C., Iyengar, S. S., Tomasi, J., Cossi, M., Millam, J. M., Klene, M., Adamo, C., Cammi, R., Ochterski, J. W., Martin, R. L., Morokuma, K., Farkas, O., Foresman, J. B., and Fox, D. J. (2016) Gaussian 16 Rev. A.03, Wallingford, CT.
- (41) Becke, A. D. (1993) Density-functional thermochemistry. III. The role of exact exchange, *The Journal of Chemical Physics* 98, 5648-5652.
- (42) Stephens, P. J., Devlin, F. J., Chabalowski, C. F., and Frisch, M. J. (1994) Ab Initio Calculation of Vibrational Absorption and Circular Dichroism Spectra Using Density Functional Force Fields, *The Journal of Physical Chemistry* 98, 11623-11627.
- (43) Thöing, C., Pfeifer, A., Kakorin, S., and Kottke, T. (2013) Protonated triplet-excited flavin resolved by step-scan FTIR spectroscopy: implications for photosensory LOV domains, *Phys. Chem. Chem. Phys.* 15, 5916-5926.
- (44) Spexard, M., Immeln, D., Thöing, C., and Kottke, T. (2011) Infrared spectrum and absorption coefficient of the cofactor flavin in water, *Vib. Spectrosc.* 57, 282-287.
- (45) Zheng, X., Garcia, J., and Stuchebrukhov, A. A. (2008) Theoretical Study of Excitation Energy Transfer in DNA Photolyase, *The Journal of Physical Chemistry B* 112, 8724-8729.
- (46) Tamada, T., Kitadokoro, K., Higuchi, Y., Inaka, K., Yasui, A., de Ruyter, P. E., Eker, A. P., and Miki, K. (1997) Crystal structure of DNA photolyase from *Anacystis nidulans*, *Nat. Struct. Biol.* 4, 887-891.
- (47) Kim, S. T., Heelis, P. F., Okamura, T., Hirata, Y., Mataga, N., and Sancar, A. (1991) Determination of rates and yields of interchromophore (folate-->flavin) energy transfer and intermolecular (flavin-->DNA) electron transfer in *Escherichia coli* photolyase by time-resolved

- fluorescence and absorption spectroscopy, *Biochemistry* 30, 11262-11270.
- (48) Rieff, B., Mathias, G., Bauer, S., and Tavan, P. (2011) Density functional theory combined with molecular mechanics: the infrared spectra of flavin in solution, *Photochem. Photobiol.* 87, 511-523.
- (49) Martin, C. B., Tsao, M.-L., Hadad, C. M., and Platz, M. S. (2002) The Reaction of Triplet Flavin with Indole. A Study of the Cascade of Reactive Intermediates Using Density Functional Theory and Time Resolved Infrared Spectroscopy, *Journal of the American Chemical Society* 124, 7226-7234.
- (50) Takahashi, R., Okajima, K., Suzuki, H., Nakamura, H., Ikeuchi, M., and Noguchi, T. (2007) FTIR study on the hydrogen bond structure of a key tyrosine residue in the flavin-binding blue light sensor TePixD from *Thermosynechococcus elongatus*, *Biochemistry* 46, 6459-6467.
- (51) Iwata, T., Zhang, Y., Hitomi, K., Getzoff, E. D., and Kandori, H. (2010) Key Dynamics of Conserved Asparagine in a Cryptochrome/Photolyase Family Protein by Fourier Transform Infrared Spectroscopy, *Biochemistry* 49, 8882-8891.
- (52) Immeln, D., Weigel, A., Kottke, T., and Pérez Lustres, J. L. (2012) Primary events in the blue light sensor plant cryptochrome: intraprotein electron and proton transfer revealed by femtosecond spectroscopy, *J. Am. Chem. Soc.* 134, 12536-12546.
- (53) Kim, S. T., Heelis, P. F., and Sancar, A. (1992) Energy transfer (deazaflavin-->FADH2) and electron transfer (FADH2 -->T<>T) kinetics in *Anacystis nidulans* photolyase, *Biochemistry* 31, 11244-11248.
- (54) Mittag, M., Kiaulehn, S., and Johnson, C. H. (2005) The circadian clock in *Chlamydomonas reinhardtii*. What is it for? What is it similar to?, *Plant Physiol.* 137, 399-409.
- (55) Mohamed, A. E., Ahmed, F. H., Arulmozhiraja, S., Lin, C. Y., Taylor, M. C., Krausz, E. R., Jackson, C. J., and Coote, M. L. (2016) Protonation state of F420H2 in the prodrug-activating deazaflavin dependent nitroreductase (Ddn) from *Mycobacterium tuberculosis*, *Molecular BioSystems* 12, 1110-1113.
- (56) Bashiri, G., Perkowski, E. F., Turner, A. P., Feltcher, M. E., Braunstein, M., and Baker, E. N. (2012) Tat-Dependent Translocation of an F420-Binding Protein of *Mycobacterium tuberculosis*, *PLOS ONE* 7, e45003.
- (57) Reichardt, C. (1994) Solvatochromic Dyes as Solvent Polarity Indicators, *Chemical Reviews* 94, 2319-2358.
- (58) Saxena, C., Wang, H., Kavakli, I. H., Sancar, A., and Zhong, D. (2005) Ultrafast dynamics of resonance energy transfer in cryptochrome, *J. Am. Chem. Soc.* 127, 7984-7985.
- (59) Tan, C., Guo, L., Ai, Y., Li, J., Wang, L., Sancar, A., Luo, Y., and Zhong, D. (2014) Direct Determination of Resonance Energy Transfer in Photolyase: Structural Alignment for the Functional State, *The Journal of Physical Chemistry A* 118, 10522-10530.

- (60) Kort, R., Komori, H., Adachi, S.-i., Miki, K., and Eker, A. (2004) DNA apophotolyase from *Anacystis nidulans*: 1.8 Å structure, 8-HDF reconstitution and X-ray-induced FAD reduction, *Acta Crystallographica Section D* *60*, 1205-1213.
- (61) Coesel, S., Mangogna, M., Ishikawa, T., Heijde, M., Rogato, A., Finazzi, G., Todo, T., Bowler, C., and Falciatore, A. (2009) Diatom PtCPF1 is a new cryptochrome/photolyase family member with DNA repair and transcription regulation activity, *EMBO Rep.* *10*, 655-661.
- (62) García-Esquivel, M., Esquivel-Naranjo, E. U., Hernández-Onate, M. A., Ibarra-Laclette, E., and Herrera-Estrella, A. (2016) The *Trichoderma atroviride* cryptochrome/photolyase genes regulate the expression of *blr1*-independent genes both in red and blue light, *Fungal Biol.* *120*, 500-512.
- (63) Heijde, M., Zabulon, G., Corellou, F., Ishikawa, T., Brazard, J., Usman, A., Sanchez, F., Plaza, P., Martin, M., Falciatore, A., Todo, T., Bouget, F. Y., and Bowler, C. (2010) Characterization of two members of the cryptochrome/photolyase family from *Ostreococcus tauri* provides insights into the origin and evolution of cryptochromes, *Plant Cell Environ.* *33*, 1614-1626.
- (64) Selby, C. P., andancar, A. (2006) A cryptochrome/photolyase class of enzymes with single-stranded DNA-specific photolyase activity, *Proc. Natl. Acad. Sci. U. S. A.* *103*, 17696-17700.
- (65) Pokorny, R., Klar, T., Hennecke, U., Carell, T., Batschauer, A., and Essen, L. O. (2008) Recognition and repair of UV lesions in loop structures of duplex DNA by DASH-type cryptochrome, *Proc. Natl. Acad. Sci. U. S. A.* *105*, 21023-21027.

For Table of Contents Only:

